



This is a repository copy of *Comparison of independent evolutionary origins reveals both convergence and divergence in the metabolic mechanisms of symbiosis.*

White Rose Research Online URL for this paper:
<http://eprints.whiterose.ac.uk/153912/>

Version: Accepted Version

Article:

Sørensen, M.E.S., Wood, A.J., Minter, E.J.A. et al. (3 more authors) (2020) Comparison of independent evolutionary origins reveals both convergence and divergence in the metabolic mechanisms of symbiosis. *Current Biology*, 30 (2). 328-334.e4. ISSN 0960-9822

<https://doi.org/10.1016/j.cub.2019.11.053>

Article available under the terms of the CC-BY-NC-ND licence
(<https://creativecommons.org/licenses/by-nc-nd/4.0/>).

Reuse

This article is distributed under the terms of the Creative Commons Attribution-NonCommercial-NoDerivs (CC BY-NC-ND) licence. This licence only allows you to download this work and share it with others as long as you credit the authors, but you can't change the article in any way or use it commercially. More information and the full terms of the licence here: <https://creativecommons.org/licenses/>

Takedown

If you consider content in White Rose Research Online to be in breach of UK law, please notify us by emailing eprints@whiterose.ac.uk including the URL of the record and the reason for the withdrawal request.



eprints@whiterose.ac.uk
<https://eprints.whiterose.ac.uk/>

Comparison of independent evolutionary origins reveals both convergence and divergence in the metabolic mechanisms of symbiosis

Megan E. S. Sørensen¹, A. Jamie Wood², Ewan J. A. Minter¹, Chris D. Lowe³,
Duncan D. Cameron¹, Michael A. Brockhurst¹

1. Department of Animal and Plant Sciences, University of Sheffield, Sheffield S10
2TN, UK

2. Department of Biology, University of York, York YO10 5DD, UK

3. Centre for Ecology and Conservation, University of Exeter, Penryn Campus,
Cornwall TR10 9FE, UK

Lead contact Michael Brockhurst (m.brockhurst@sheffield.ac.uk)

1 **Summary**

2 Through the merger of once independent lineages, symbiosis promotes the
3 acquisition of new traits and the exploitation of inaccessible ecological niches [1,2],
4 driving evolutionary innovation and important ecosystem functions [3–6]. The
5 transient nature of establishment makes study of symbiotic origins difficult, but
6 experimental comparison of independent originations could reveal the degree of
7 convergence in the underpinning mechanisms [7,8]. We compared the metabolic
8 mechanisms of two independent origins of the *Paramecium bursaria-Chlorella*
9 photosymbiosis [9–11] using a reciprocal metabolomic pulse-chase method. This
10 showed convergent patterns of nutrient exchange and utilisation for host-derived
11 nitrogen in the *Chlorella* genotypes [12,13] and symbiont-derived carbon in the *P.*
12 *bursaria* genotypes [14,15]. Consistent with a convergent primary nutrient exchange,
13 partner-switched host-symbiont pairings were functional. Direct competition of hosts
14 containing native or recombined symbionts against isogenic symbiont-free hosts
15 showed that the fitness benefits of symbiosis for hosts increased with irradiance but
16 varied by genotype. Global metabolism varied more between the *Chlorella* than the
17 *P. bursaria* genotypes, and suggested divergent mechanisms of light management.
18 Specifically, the algal symbiont genotypes either produced photo-protective
19 carotenoid pigments at high irradiance or more chlorophyll, resulting in
20 corresponding differences in photosynthetic efficiency and non-photochemical
21 quenching among host-symbiont pairings. These data suggest that the multiple
22 origins of the *P. bursaria-Chlorella* symbiosis use a convergent nutrient exchange,
23 whereas other photosynthetic traits linked to the functioning of the photosymbiosis
24 have diverged. While convergence enables partner-switching among diverse strains,

25 phenotypic mismatches resulting from divergence of secondary-symbiotic traits could
26 mediate host-symbiont specificity in nature.

27

28 **Results and Discussion**

29 Independent evolutionary origins of a beneficial symbiotic relationship suggests that
30 a strong selective advantage has, on multiple occasions, overcome the inherent
31 conflict between the self-interest of the partners [16,17]. Independent origins of
32 symbiosis appear to be common and have been reported in diverse symbiotic
33 relationships [18–21]. Experimental comparison of independent origins could reveal
34 the degree of convergence versus divergence in the underpinning mechanisms [7,8].
35 A convergent nutrient exchange would suggest evolutionary constraint and limited
36 viable routes to symbiosis, but may allow partner-switching between independent
37 lineages, whereas divergence would tend to drive host-symbiont specificity. Here we
38 use the experimentally tractable microbial symbiosis between the heterotrophic
39 ciliate *Paramecium bursaria* and the photosynthetic green alga *Chlorella* sp [9].
40 These species engage in a facultative photosymbiosis that is widely distributed in
41 freshwater habitats [22], wherein ~100-600 algal cells live inside a ciliate cell and
42 provide products of photosynthesis in exchange for organic nitrogen [14,23]. This
43 symbiotic interaction has originated multiple times and forms two distinct
44 biogeographical clades, specifically, the European clade and the American/Japanese
45 clade [10,11]. Using a representative of each clade [the strain 186b originally
46 isolated in the UK and strain HA1 originally isolated in Japan (Table S1); clade
47 identity was confirmed by diagnostic PCR (Figure S1)] we first tested whether these
48 strains used convergent biochemical mechanisms of carbon (from the photosynthetic
49 endosymbiotic *Chlorella*) for nitrogen (acquired by the protist host though the

50 ingestion and digestion of free-living bacteria) exchange [14]. To do this, we devised
51 a reciprocal, temporally-resolved, metabolomic pulse chase experiment that
52 simultaneously monitored nitrogen and carbon assimilation in the symbiont and host,
53 respectively. Specifically, using ^{15}N -labelled bacterial necromass, we traced isotopic
54 enrichment derived from N assimilated through *P. bursaria* digestion in *Chlorella*
55 metabolites. In parallel, using ^{13}C -labelled HCO_3^- we traced isotopic enrichment
56 derived from C fixed by *Chlorella* photosynthesis in *P. bursaria* metabolites. The
57 quantity of every individual metabolite in each sample was determined using Liquid
58 Chromatography Time of Flight Mass Spectrometry (LC-ToFMS). This allowed the
59 metabolic fate of resources exchanged between symbiotic partners to be quantified
60 over time, allowing comparison of symbiotic metabolism between the strains.

61

62 We used Random Forest models, a form of computational learning involving the
63 construction of an extensive array of possible compatible decision trees, to identify
64 which metabolites were associated with isotopic enrichment. Among *Chlorella*
65 metabolites we observed a shared ^{15}N isotopic enrichment response among strains
66 (i.e. high-ranking score in both strains) in 46% of all metabolites (78 % of nitrogen-
67 containing metabolites), suggesting that both *Chlorella* strains directed the
68 exchanged nitrogen through metabolism in similar ways (Figure 1). Similarly, we
69 observed a shared ^{13}C enrichment response in 75 % of *P. bursaria* metabolites (78%
70 of carbon-containing metabolites), suggesting a high degree of convergence
71 between the *P. bursaria* host strains in how they utilised the C derived from their
72 algal symbionts (Figure 1). The pattern of shared enrichment among strains was
73 consistently high for both ^{15}N and ^{13}C isotopic enrichment across all sampled time-
74 points, suggesting a conserved nutrient exchange (Figure 1). Smaller proportions of

75 metabolites showed an asymmetric response (i.e., were high-ranked in one strain
76 but low-ranked in the other; for ^{15}N enrichment, 20.55% in 186b *Chlorella* and 9.55%
77 in HA1 *Chlorella*; for ^{13}C enrichment 13.17% in 186b *P. bursaria* and 3.42% in HA1
78 *P. bursaria*), suggesting only limited divergence in utilisation of exchanged
79 metabolites has occurred between these host-symbiont clades.

80

81 Co-enriched metabolites with the strongest enrichment over time were identified
82 using LC-ToFMS (simultaneously resolving the monoisotopic mass and
83 chromatographic retention time for each M/Z). For ^{15}N co-enrichment in *Chlorella*
84 (Table S2), we identified metabolites associated with the amino acid and purine
85 pathways, which have both previously been suggested as probable N exchange
86 metabolites in this symbiosis [12,24–27]. Targeted analyses of these pathways were
87 used to calculate the enrichment dynamics in the constituent metabolites. These
88 dynamics indicated that an amino acid is the more likely N exchange metabolite from
89 *P. bursaria* to *Chlorella* in both clades. Although our first sampling time-point was not
90 early enough to permit direct observation of metabolite exchange itself, downstream
91 enrichment profiles suggest that the most likely candidate exchange metabolite is
92 arginine (see Figure S4), an amino acid known to support growth of *Chlorella* as its
93 sole N source [28]. In addition, we observed co-enrichment in larger, N-rich
94 metabolites, including chlorophyll precursors, which most likely represent the largest
95 N-sinks for *Chlorella*, thus becoming enriched in ^{15}N as a function of N demand. For
96 ^{13}C enrichment in *P. bursaria* (Table S3), we identified metabolites involved in
97 carbohydrate and lipid metabolism, suggesting that symbiont derived C was directed
98 to carbon storage, as well as enrichment in central and amino acid metabolism,
99 which are likely to have a high turnover of carbon and represent strong carbon sinks.

100 For some carbohydrate storage metabolites, we observed stronger differences in ¹³C
101 enrichment between light conditions in the 186b compared to the HA1 strain (Figure
102 S3), indicating strain differences in the rate of flux through some of co-enriched
103 pathways.

104

105 The pulse-chase analysis suggests that these *P. bursaria-Chlorella* strains,
106 representing independent origins of the symbiosis, show convergent utilisation of
107 partner-derived nutrients, and we hypothesised therefore that partner-switched host-
108 symbiont pairings would be functional. To test this, we performed a reciprocal cross-
109 infection experiment whereby the *P. bursaria* host strains were cured of their native
110 algal symbiont, and subsequently re-infected with either their native algal symbiont
111 or the reciprocal non-native algal symbiont. We then directly competed each host-
112 symbiont pairing against its respective symbiont-free host strain across a light
113 gradient. Note that reinfection of aposymbiotic host populations by symbionts occurs
114 over far longer timescales (i.e. several weeks) than the competition assay, such that
115 this process is unlikely to affect relative fitness estimates. We used flow cytometry to
116 quantify the proportion of green (with symbiont) versus white (symbiont-free) host
117 cells at the start and end of the growth cycle to calculate the selection rate [23], thus
118 providing a direct measure of the fitness effect of symbiosis for hosts. All the
119 symbiont pairings showed a classic photosymbiotic reaction norm, such that the
120 relative fitness of hosts with symbionts versus hosts without symbionts increased
121 with increasing irradiance (Figure 2), and more steeply in the HA1 host background
122 (host genotype by light environment interaction, ANOVA, $F_{3,31} = 29.34$, $P < 0.001$).
123 This confirms that both host genotypes could derive the benefits of symbiosis from

124 either of the symbiont genotypes, but that the fitness effect of symbiosis varied
125 between strains.
126
127 These light-dependent differences in the fitness of the host-symbiont pairings
128 suggest that the HA1 and 186b strains may have diverged in aspects of their
129 metabolism and physiology besides the primary symbiotic nutrient exchange. To
130 characterise potential differences in global metabolism between the HA1 and 186b
131 host-symbiont strains, we performed untargeted metabolomics analyses on the
132 unlabelled metabolites from the separated *Chlorella* and *P. bursaria* fractions of both
133 the native host-symbiont pairings. We observed a range of metabolites that
134 differentiated the 186b and HA1 *Chlorella* strains (Table S4), and metabolism
135 differed more between strains than it did between light conditions within strains
136 (Figure 3 panels A-D). Notably, the HA1 *Chlorella* strain displayed higher levels of
137 several carotenoids than the 186b *Chlorella* strain, particularly at high irradiance,
138 whereas the 186b *Chlorella* strain displayed higher levels of metabolites involved in
139 chlorophyll and ubiquinol metabolism than the HA1 *Chlorella* strain at both low and
140 high irradiance (Figure 3 panels E-J). Fewer metabolites distinguished the global
141 metabolism of the *P. bursaria* strains (Table S4). In all cases these metabolites were
142 present at higher levels in the 186b *P. bursaria* strain compared to the HA1 *P.*
143 *bursaria* strain (Figure S2), and neither strain's metabolism varied significantly with
144 irradiance (Figure S2). The identified metabolites that distinguished the strains were
145 associated with a range of functions, including amino acid metabolism, amino
146 sugars, and sphingolipid metabolism. Several other metabolites, although present in
147 the host fraction, are likely to have been secreted into the host cytoplasm by the
148 algal symbiont or be derived from the bacterial necromass. These include a zeatin

149 candidate, which may play a role in *Chlorella* signalling, and several metabolites
150 identified as putative antibiotics.

151

152 The clear differences in global metabolism between the algal strains suggests that
153 they may vary in their photophysiology. To test this, we measured several key
154 photochemical parameters in the native and partner-switched host-symbiont pairings
155 acclimated to a range of light levels. For two measures of photosynthetic efficiency
156 — F_v/F_m (the intrinsic efficiency of photosystem II [PSII], Figure 4A) and Φ_{PSII} (the
157 proportion of the light absorbed by chlorophyll associated with PSII that is used in
158 photochemistry, Figure 4B) [29] — we observed a significant host genotype by
159 symbiont genotype by light environment interaction [for F_v/F_m ANOVA, $F_{7,232} = 86.41$,
160 $P < 0.001$; for Φ_{PSII} nlme model intercept summary ANOVA, $F_{11,24} = 11.66$, $P < 0.001$
161 (see Data S1 for full statistical output)]. In the HA1 *P. bursaria* host, the pattern of
162 photosynthetic efficiency across the light gradient did not vary with algal strain,
163 whereas in the 186b *P. bursaria* host, the native 186b *Chlorella* showed lower
164 photosynthetic efficiency than the HA1 *Chlorella* at low growth irradiance, but the
165 pattern was reversed at high growth irradiance. These patterns are consistent with
166 the observed differences in carotenoid metabolism among the *Chlorella* strains: The
167 HA1 *Chlorella* produced more carotenoids at high irradiance than the 186b *Chlorella*;
168 because carotenoids perform a role in photoprotection they can therefore decrease
169 the light energy that reaches the photosystems thus limiting photosynthesis.

170

171 Non-photochemical quenching is used by photosynthetic organisms to safely deal
172 with excess and potentially damaging light energy and was estimated using the
173 normalised Stern-Volmer coefficient (NSV). The intercept of the NSV response

174 (Figure 4C) across the actinic light gradient was significantly affected by host
175 genotype, suggesting differences among the host genotypes in their ability to photo-
176 protect algal symbionts (ANOVA, $F_{1,34} = 4.74$, $P < 0.05$). Meanwhile, both symbiont
177 genotype and growth irradiance affected the first coefficient (ANOVA, $F_{3,32} = 5.56$,
178 $P < 0.01$); and symbiont genotype affected the second coefficient (ANOVA, $F_{1,34} =$
179 8.932 , $P < 0.01$) (see Data S1 for full statistical output). Higher levels of NSV and
180 steeper NSV reaction norms for the 186b *Chlorella*, particularly in its native host
181 background, are consistent with the greater investment in photosynthetic machinery
182 observed in the metabolome, allowing this genotype to better dissipate excess light
183 energy as heat whilst not compromising photosynthetic efficiency.

184

185 Mixotrophic photosymbioses are common and play a vital role in biogeochemical
186 cycling in terrestrial and aquatic ecosystems [30–32]. Their breakdown, often driven
187 by environmental change, can be rescued by partner-switching to restore symbiotic
188 function [33,34]. Our findings suggest that convergence among independent
189 symbiotic origins upon a shared primary symbiotic nutrient exchange enables
190 partner-switching between genetically divergent clades. This stands in contrast to the
191 diversity of exchange metabolites used in photosymbioses more broadly. For
192 example, just amongst photosymbiotic cnidaria (i.e. corals, anemones, jellyfish)
193 organic carbon transfer from symbiont to host occurs in the form of glycerol, glucose,
194 maltose, and a variety of lipids and amino acids [35]. Thus, while a variety of
195 potential metabolic solutions to the photosymbiotic nutrient exchange exist, perhaps
196 explaining the abundance and diversity of photosymbioses, within specific symbiotic
197 interactions the optimal solution may be more constrained, resulting in evolutionary
198 convergence among independent originations. The concurrent divergence in algal

199 photophysiology allowed hosts, through partner-switching, to acquire symbionts with
200 different properties, potentially enabling adaptation to new environments. Crucially,
201 symbiont replacement providing hosts with new adaptive traits is critical in natural
202 populations responding to environmental change; for example, reinfection of corals
203 by thermally tolerant symbionts enables recovery following thermal bleaching events
204 [36–38]. Finally, we observed differences among the *P. bursaria-Chlorella* clades in
205 their division of labour between host and symbiont contributions to photoprotection.
206 This may be a common feature of photosymbioses [39,40], for example some
207 pelagic zooplankton and jellyfish hosts adopt behavioural strategies to photoprotect
208 algal symbionts [41], and could be a key mechanism of host-symbiont specificity by
209 mediating genotype by genotype by environment interactions. Host-symbiont
210 specificity and partner-switching are common features of many symbioses [42–46]
211 suggesting that our findings are likely to be of wider relevance beyond
212 photosymbioses. Multiple independent evolutionary origins have occurred in diverse
213 symbiotic relationships [18–21]. While this suggests a strong selective imperative for
214 these symbioses, it may also provide important adaptive potential through functional
215 divergence among originations enabling their resilience to environmental change.

216

217 **Acknowledgements**

218

219 This work was funded by grant NE/K011774/2 from the Natural Environment
220 Research Council, UK to MAB, CDL, DDC, and AJW, and a White Rose DTP
221 studentship from the Biotechnology and Biological Sciences Research Council, UK
222 to MESS (BB/M011151/1). The funders had no role in the design of the study, the

223 collection, analysis and interpretation of data, or the writing of the manuscript. We
224 are grateful to Heather Walker for assistance.

Author contributions

225 MB, DC, MS, EM, CL conceived and designed the study. MS and EM conducted
226 experimental work. MS, CL and DC analysed the data. MS and MB drafted the
227 manuscript. All authors commented on the manuscript.

Declaration of Interests

228 The authors declare that they have no conflicting interests.

229

230

231

232

233

234

235

236

237

238

239 **Figure Legends**

240

241 **Figure 1: Correlated metabolite enrichment for the 186b and HA1 *Paramecium***
242 ***bursaria* and *Chlorella* strains over time.**

243 Each data point represents a metabolite. In each scatterplot the mean Random

244 Forest rank order of each metabolite in the HA1 strain is plotted against the mean

245 rank order of each metabolite in the 186b strain. The rank order value is positively

246 correlated with magnitude of the enrichment signal. For all panels, the mean rank

247 order is derived from multiple Random Forest analyses (n=500), for further details

248 regarding the Random Forest models see the methods section. A,C,E,G.) ¹⁵N

249 enrichment in the *Chlorella* fraction at 15, 120, 240 and 360 minutes. B,D,F,H.) ¹³C

250 enrichment in the *P. bursaria* fraction at 15, 120, 240 and 360 minutes. See Table S2

251 for the identified metabolites associated with ¹⁵N enrichment in both *Chlorella* strains;

252 and see Table S3 for the identified metabolites associated with ¹³C enrichment in

253 both *Paramecium* strains.

254

255 **Figure 2: Fitness of the native and non-native host-symbiont pairings relative**
256 **to isogenic symbiont-free hosts.**

257 Lines show mean (n=3) competitive fitness of symbiont-containing hosts relative to

258 their isogenic symbiont-free host genotype calculated as selection rate, the shaded

259 area denotes \pm SE. The left-hand panel shows data for the HA1 *Paramecium* host

260 genotype, the right-hand panel shows data for the 186b *Paramecium* host genotype

261 containing either native (solid line) or non-native (dashed line) *Chlorella* symbiont

262 genotypes, which are distinguished by colour (186b *Chlorella* in blue; HA1 *Chlorella*

263 in green). Selection rate = 0 represents equal fitness. See Data S1 for details on the
264 statistics used.

265

266

267 **Figure 3: Differences in *Chlorella* global metabolism between strains across**
268 **light conditions.**

269 Comparisons of unlabelled *Chlorella* metabolites between strains and light conditions
270 are represented as volcano plots (A-D) plotting the fold change of each metabolite
271 against its statistical significance. The data points are highlighted at two false
272 discovery rate (FDR) values, and if the $\text{Log}_2(\text{fold change})$ is greater than 1 or less
273 than -1 as indicated in the graphical key. A.) Comparing metabolites between the two
274 strains within the high light condition. B.) Comparing metabolites between the two
275 strains within the low light condition. C.) Comparing metabolites between the two
276 light levels within the HA1 strain. D.) Comparing metabolites between the two light
277 levels within the 186b strain. See Figure S2 for the equivalent plot for the *P. bursaria*
278 metabolite comparisons and see Table S4 for the identified metabolites. Differential
279 metabolites distinguishing the divergent strategies of light management between the
280 two host-symbiont strains were then plotted separately: The relative abundance of
281 the metabolites is plotted within the two strains at the two light conditions. The top
282 three panels (E-G) show metabolites that have been identified as carotenoids and
283 the lower three panels (H-J) show metabolites that have been identified as either
284 chlorophyll or ubiquinone compounds. For panels E-J, responses are presented as
285 the mean ($n=12$) \pm SE and host-symbiont strain is denoted by colour (186b in blue;
286 HA1 in green).

287

288 **Figure 4: Photophysiology measurements for the native and non-native host-**
289 **symbiont pairings.**

290 For all subplots, lines represent the mean (n=3), the shaded area denotes \pm SE. In
291 each subplot the left-hand panel shows data for the HA1 *Paramecium* host
292 genotype, the right-hand panel shows data for the 186b *Paramecium* host genotype
293 containing either native (solid line) or non-native (dashed line) *Chlorella* symbiont
294 genotypes, which are distinguished by colour (186b *Chlorella* in blue; HA1 *Chlorella*
295 in green). A) Estimates of the maximum quantum yield of photosystem II (F_v/F_m)
296 across growth irradiances. B) Light-adapted quantum yield of photosystem II (Φ_{PSII})
297 across growth irradiances, lines represent exponential decay models using nlme
298 package in R. C.) The normalised Stern-Volmer quenching coefficient ($NSV = F_o'/F_v'$)
299 across growth irradiances, presented at polynomial model fits. See Data S1 for
300 details on the statistics used.

301

302 **STAR Methods**

303 LEAD CONTACT AND MATERIALS AVAILABILITY

304 Further information and requests for resources and reagents should be directed to
305 and will be fulfilled by the Lead Contact, Michael Brockhurst
306 (m.brockhurst@sheffield.ac.uk). The HA1 and 186b *Paramecium bursaria* strains
307 used in this study will be made available upon request but can also be obtained from
308 national culture collections (detailed below).

309

310 EXPERIMENTAL MODEL AND SUBJECT DETAILS

311

312 Symbiotic *Paramecium bursaria* stock cultures were maintained at 25°C under a
313 14:10 L:D cycle with 50 $\mu\text{E m}^{-2} \text{s}^{-1}$ of light. Grown in bacterized Protozoan Pellet
314 Media (PPM, Carolina Biological Supply), made to a concentration of 0.66 g L⁻¹ with
315 Volvic natural mineral water, and inoculated approximately 20 hours prior to use with
316 *Serratia marscesens* from frozen glycerol stocks. The two natural strains used were:
317 186b (CCAP 1660/18) obtained from the Culture Collection for Algae and Protozoa
318 (Oban, Scotland), and HA1 isolated in Japan and obtained from the Paramecium
319 National Bio-Resource Project (Yamaguchi, Japan). Further details regarding these
320 strains and the habitats they were isolated from can be found in Table S1.

321

322 To isolate *Chlorella* from the symbiosis, symbiotic cultures were first washed and
323 concentrated with a 11 μm nylon mesh using sterile Volvic. The suspension was then
324 ultra-sonicated using a Fisherbrand™ Q500 Sonicator (Fisher Scientific, NH, USA),
325 at a power setting of 20% for 10 seconds sonification to disrupt the host cells. The
326 liquid was then spotted onto Bold Basal Media plates (BBM) [47], from which green

327 colonies were streaked out and isolated over several weeks. Plate stocks were
328 maintained by streaking out one colony to a fresh plate every 3/4 weeks.

329

330 Symbiont-free *P. bursaria* were made by treating symbiotic cultures with paraquat
331 ($10 \mu\text{g mL}^{-1}$) for 3 to 7 days in high light conditions ($>50 \mu\text{E m}^{-2} \text{s}^{-1}$), until the host
332 cells were visibly symbiont free. The cultures were then extensively washing with
333 Volvic and closely monitored with microscopy to check that re-greening by *Chlorella*
334 did not occur. Stock cultures of the symbiont-free cells were maintained by batch
335 culture at 25°C under a 14:10 L:D cycle with $3 \mu\text{E m}^{-2} \text{s}^{-1}$ of light and were given fresh
336 PPM weekly.

337

338 METHOD DETAILS

339

340 *Cross Infections*

341 Symbiont-free populations of the two *P. bursaria* strains were re-infected by adding a
342 colony of *Chlorella* from the plate stocks derived from the appropriate strain. The re-
343 greening process was followed by microscopy and took between 2-6 weeks. Over
344 the process, cells were grown at the intermediate light level of $12 \mu\text{E m}^{-2} \text{s}^{-1}$ and
345 were given bacterized PPM weekly.

346

347 *Diagnostic PCR*

348 The correct algae genotype was confirmed using diagnostic PCR (see Figure S1).

349 The *Chlorella* DNA was extracted by isolating the *Chlorella* and then using a
350 standard 6% Chelex100 resin (Bio-Rad) extraction method. ISSR primer '65' were
351 established for *Chlorella vulgaris* by Shen [48], and was used as described therein.

352 Standard PCR reactions were performed using Go Taq Green Master Mix (Promega)

353 and 0.5 μ mol L⁻¹ of primer. The thermocycler programme was set to: 94 $^{\circ}$ c for 5min,
354 40 cycles of (94 $^{\circ}$ c for 20sec, 55 $^{\circ}$ c for 1 min, 72 $^{\circ}$ c for 20sec), and 6 min at 72 $^{\circ}$ c.

355

356 *Fitness assay*

357 *P. bursaria* cultures, both the symbiotic cross-infections and symbiont-free cells,
358 were washed with Volvic and resuspended in bacterized PPM. The cultures were
359 then split and acclimated at their treatment light level (0,12,50 μ E m⁻² s⁻¹) for five
360 days. Cell densities were counted by fixing 360 μ L of each cell culture, in triplicate, in
361 1% v/v glutaraldehyde in 96-well flat bottomed micro-well plates. Images were taken
362 with a plate reader (Tecan Spark 10M) and cell counts were made using an
363 automated image analysis macro in ImageJ v1.50i [49]. The competitions were
364 started with the target values of 20 green cells and 20 white cells per ml. Cells were
365 sampled on day 0 and day 7 and the proportion of green to white cells was
366 measured using flow cytometry analysis. Green versus white cells were
367 distinguished using single cell fluorescence estimated using a CytoFLEX S flow
368 cytometer (Beckman Coulter Inc., CA, USA) by measuring the intensity of chlorophyll
369 fluorescence (excitation 488nm, emission 690/50nm) and gating cell size using
370 forward side scatter [23]. The measurements were calibrated against 8-peak rainbow
371 calibration particles (BioLegend), and then presented as relative fluorescence to
372 reduce variation across sampling sessions. See Data S1 for details on the statistics
373 used to analysis the fitness assay.

374

375 *Fluorimetry*

376 The cells were washed and concentrated with a 11 μ m nylon mesh using sterile
377 Volvic and re-suspended in bacterized PPM. The cultures were then split and

378 acclimated to their treatment light condition ($12, 24 \text{ \& } 50 \mu\text{E m}^{-2} \text{ s}^{-1}$) for five days.
379 F_v/F_m , Φ_{PSII} , and NSV values were measured by fast repetition rate fluorimetry
380 (FastPro8, Chelsea instruments fluorometer [50] following the manufacturer's
381 procedure). Cultures were dark acclimated for 15 minutes prior to measurements.
382 For maximum quantum yield, measurements were repeated until F_v/F_m stabilized
383 (typically 3-5minutes) and F_v/F_m then estimated as an average of 10 measurements.
384 Φ_{PSII} was measured in response to an actinic light source at sequentially increasing
385 irradiances between 0 – 2908 PFD following standard green algae protocol. Peak
386 emission wavelengths of the LED used for excitations was 450nm. Non-
387 photochemical quenching was estimated by the normalised Stern-Volmer coefficient,
388 defined as $\text{NSV} = F_o'/F_v'$ [51] and corrects for differences in F_v/F_m between samples.
389 See Data S1 for details on the statistics used to analysis the fluorimetry results.

390

391 *Metabolomics*

392 Cultures were washed and concentrated with a $11\mu\text{m}$ nylon mesh using Volvic and
393 re-suspended in bacterized PPM. The cultures were first grown for three days at 50
394 $\mu\text{E m}^{-2} \text{ s}^{-1}$ to increase cell densities, and then split and acclimated at their treatment
395 light condition ($6 \text{ \& } 50 \mu\text{E m}^{-2} \text{ s}^{-1}$) for three days. For the sampling, the cultures were
396 split into 3 treatment: the control, N^{15} enrichment by the addition of labelled *Serratia*
397 *marcescens* ($100\mu\text{l}$ per microcosm), or C^{13} enrichment by the addition of HC^{13}O_3
398 (100 mg L^{-1}). The cultures were sampled at four time points (15, 120, 360, 480
399 minutes after the enrichment event). There were three biological replicates for each
400 sampling event.

401

402 At each sampling event, the symbiotic partners were separated in order to get *P.*
403 *bursaria* and *Chlorella* metabolic fraction. The *P. bursaria* cells were concentrated
404 with a 11µm nylon mesh using Volvic and then the *P. bursaria* cells were disrupted
405 by sonication (20% power for 10 secs). 1ml of the lysate was pushed through a
406 1.6µm filter, which caught the intact *Chlorella* cells, and the run-through was
407 collected and stored as the *P. bursaria* fraction. The 1.6µm filter was washed with
408 5ml cold deionized water, and then reversed so that the *Chlorella* cells were
409 resuspended in 1ml of cold methanol, which was stored as the *Chlorella* fraction.

410

411 The samples were analysed with a Synapt G2-Si with Acquity UPLC, recording in
412 positive mode over a large untargeted mass range (50 – 1000 Da). A 2.1x50mm
413 Acquity UPLC BEH C18 column was used with acetonitrile as the solvent. The
414 machine settings are listed in detail below:

415

416 Mass spectrometry settings:

417	Polarity:	positive
418	Capillary voltage:	2.3 kV
419	Sample Cone voltage:	20 V
420	Source Temperature:	100°C
421	Desolvation temperature:	280°C
422	Gas Flow:	600 L hr ⁻¹
423	Injected volume:	5µl

424

425 Gradient information:

426

427

428

429

430

Time (mins)	Water (%)	Acetonitrile (%)
0	95	5
3	65	35
6	0	100
7.5	0	100
7.6	95	5

431 The *P. bursaria* and *Chlorella* fraction were analysed separately. The xcms R
432 package [52–54] was used for automatic peak detection by extracting the spectra
433 from the CDF data files, using a step argument of 0.01 m/z. The automatically
434 identified peaks were grouped across samples and were used to identify and correct
435 correlated drifts in retention time from run to run. Pareto scaling was applied to the
436 resulting intensity matrix.

437

438 *Isotope analysis*

439 For the *P. bursaria* isotope analysis the C¹³ labelled samples were compared with
440 the control, while for the *Chlorella* analysis the N¹⁵ labelled samples were compared
441 to the control. In order to identify isotopic enrichment without user bias, we used
442 Random Forest (RF) models to identify metabolites that associated with the isotope
443 labelling. This is a machine-learning decision-tree based approach that produces
444 powerful multivariate regression and is an established method for high-throughput
445 biological data [55], including metabolomics [56]. The isotope label was used as the
446 response variable to regress against the metabolic profile of each sample. Each
447 random forest model was run with 1000 iterations, and each RF analysis was run
448 500 times to account for uncertainty in the rank score. For each run, the rank score
449 of the RF importance (measured as the mean decrease in Gini) was recorded for
450 each m/z bin. The mean and standard error of the rank score was then calculated to

451 assess the consistency of the variable importance. In total 4 RF models were
452 analysed within each fraction, 1 per timepoint.
453
454 The rank score values were then compared between the strains. The co-enriched
455 metabolites were filtered to select those that had a higher relative abundance in the
456 labelled fraction than in the control. From these, the profile of each candidate
457 metabolite was manually checked for isotopic enrichment, and when a clear
458 enrichment profile was present the monoisotopic mass was identified. The
459 enrichment proportion of the isotopic masses to the monoisotopic mass was
460 calculated, and the natural enrichment value within the control fraction was
461 subtracted from the enrichment in the labelled fraction. Following this calculation, it
462 was possible to determine if enrichment had occurred, and if so, the monoisotopic
463 mass was considered a 'mass of interest'.

464

465 *Target Pathway analysis*

466 Given that the low molecular weight compounds in the results of the ^{15}N co-
467 enrichment in *Chlorella* (Table S2) were almost exclusively amino acid or purine
468 related, we focused on these pathways for a further targeted approach. Key
469 compounds of these pathways were selected and searched for in the metabolite
470 dataset. To follow the flow of enriched nitrogen in these pathways, the relative
471 enrichment profile of these compounds compared to the control fraction was
472 calculated. The results were visualised as heatmaps, with the heatmap.2() function
473 from the gplot package [57], based on the method used by Austen et al. (In Press).
474

475 Some of the amino acid metabolism results are plotted in Figure S4 and show that
476 the nitrogen enrichment is focused downstream from arginine. Other aspects of
477 amino acid metabolism, such as that centred around aspartate, serine or lysine,
478 showed little and inconsistent enrichment. Within purine metabolism, the nitrogen
479 enrichment occurred both up and downstream of the purine bases. The enrichment
480 upstream of the purine bases indicates that enriched nitrogen is entering this
481 pathway from the amino acid of central metabolism. Based on this pattern, we
482 believe that the purine pathway is a site of secondary enrichment and it reveals that
483 purine-derivatives present a substantial nitrogen demand.

484

485 Unfortunately, we could not identify a candidate compound for arginine to test if it
486 had the enrichment profile of a transfer molecule (predicted to be a very high initial
487 enrichment that then substantially decreased over time). Such a pattern was not
488 seen for any compound, we suggest, therefore, that our first timepoint was not early
489 enough to capture the initial enrichment events involving the transfer compound
490 itself.

491

492 For ^{13}C enrichment within the *Paramecium* fraction, the results identified
493 carbohydrate metabolites (Table S3). Given that these are likely to relate to the
494 carbon transferred from the *Chlorella*, we investigated these compounds in more
495 detail, and found an interaction between light intensity and strain identity on their
496 enrichment profile (See Figure S3).

497

498 *Unlabelled analysis*

499 For the unlabelled, control fraction, metabolite relative abundance was compared
500 between the strains by calculating the log₂(Fold Change) between the conditions
501 (either between the strains within each light level, or between the light levels within
502 each strain) in a series of pair-wise contrasts for each metabolite. Student T-tests
503 were performed between the relative abundances of the paired comparisons. The
504 *Benjamini–Hochberg* procedure was used to account for the high number of multiple
505 P-value comparisons, with the false discovery rate set to 0.1 and 0.05 [58] as
506 highlighted in the volcano plots.

507

508 *Identification of significant masses*

509 Masses of interest were investigated using the MarVis-Suite 2.0 software
510 (<http://marvis.gobics.de/>) [59], using retention time and mass to compare against
511 KEGG (<https://www.genome.jp/kegg/>) [60,61] and MetaCyc (<https://biocyc.org/>) [62]
512 databases. The Metabolomics Standards Initiative requires two independent
513 measures to confirm identity, which the combination of retention time and accurate
514 mass achieves. This analysis therefore confirms level 1 identification.

515

516

517 QUANTIFICATION AND STATISTICAL ANALYSIS

518 Statistical analyses were performed in R v.3.5.0 [63] and all plots were produced
519 using package ggplot2 [64]. Physiology tests were analysed by both ANOVA and
520 ANCOVA, with light, host and symbiont identity as factors. Φ_{PSII} results were
521 analysed with non-linear mixed effects models (nlme) with the nlme R package [65].
522 The Φ_{PSII} data was fitted to an exponential decay function:

523

524

$$\Phi_{PSII} = a e^{(bl)}$$

525 Where a is a normalisation constant and b is the rate constant. The nlme model
526 included random effects for replicate on each parameter and fixed factors of host,
527 symbiont and light factors and their interactions with a following model reduction.
528 See the full statistics table (Data S1) for further details on the statistics used.

529

530 DATA AND CODE AVAILABILITY

531 The data has been deposited within Mendeley Data (DOI: 10.17632/6zspctmwpj.1).

532

533

534

535 **Legends for supplementary datasets**

536

537 **Data S1. Statistical outputs for analyses associated with the figures of the**

538 **main manuscript. Related to Figure 2 and 5**

539

540 **References:**

- 541 1. Wernegreen, J.J. (2012). Endosymbiosis. *Current Biology* 22, R555–R561.
- 542 2. Sudakaran, S., Kost, C., and Kaltenpoth, M. (2017). Symbiont Acquisition and
543 Replacement as a Source of Ecological Innovation. *Trends in Microbiology* 25, 375–390.
- 544 3. Kiers, E.T., and West, S.A. (2015). Evolving new organisms via symbiosis. *Science* 348,
545 392–394.
- 546 4. Powell, J.R., and Rillig, M.C. (2018). Biodiversity of arbuscular mycorrhizal fungi and
547 ecosystem function. *New Phytol.*
- 548 5. Baker, A.C. (2003). Flexibility and Specificity in Coral-Algal Symbiosis: Diversity,
549 Ecology, and Biogeography of Symbiodinium. *Annual Review of Ecology, Evolution,*
550 *and Systematics* 34, 661–689.
- 551 6. Zook, D.P. (2002). Prioritizing Symbiosis to Sustain Biodiversity: Are Symbionts
552 Keystone Species? In *Symbiosis: Mechanisms and Model Systems Cellular Origin, Life*
553 *in Extreme Habitats and Astrobiology.*, J. Seckbach, ed. (Dordrecht: Springer
554 Netherlands), pp. 3–12. Available at: https://doi.org/10.1007/0-306-48173-1_1.
- 555 7. Sachs, J.L., Skophammer, R.G., and Regus, J.U. (2011). Evolutionary transitions in
556 bacterial symbiosis. *PNAS* 108, 10800–10807.
- 557 8. Moran, N.A., and Wernegreen, J.J. (2000). Lifestyle evolution in symbiotic bacteria:
558 insights from genomics. *Trends in Ecology & Evolution* 15, 321–326.
- 559 9. Fujishima, M., and Kodama, Y. (2012). Endosymbionts in Paramecium. *European*
560 *Journal of Protistology* 48, 124–137.
- 561 10. Hoshina, R., and Imamura, N. (2008). Multiple Origins of the Symbioses in Paramecium
562 bursaria. *Protist* 159, 53–63.
- 563 11. Summerer, M., Sonntag, B., and Sommaruga, R. (2008). Ciliate-Symbiont Specificity of
564 Freshwater Endosymbiotic Chlorella (trebouxiophyceae, Chlorophyta)1. *Journal of*
565 *Phycology* 44, 77–84.
- 566 12. Kato, Y., Ueno, S., and Imamura, N. (2006). Studies on the nitrogen utilization of
567 endosymbiotic algae isolated from Japanese Paramecium bursaria. *Plant Science* 170,
568 481–486.
- 569 13. Kessler, E., and Huss, V. a. R. (1990). Biochemical Taxonomy of Symbiotic Chlorella
570 Strains from Paramecium and Acanthocystis*. *Botanica Acta* 103, 140–142.
- 571 14. Johnson, M.D. (2011). The acquisition of phototrophy: adaptive strategies of hosting
572 endosymbionts and organelles. *Photosynth Res* 107, 117–132.
- 573 15. Ziesenisz, E., Reisser, W., and Wiessner, W. (1981). Evidence of de novo synthesis of
574 maltose excreted by the endosymbiotic Chlorella from Paramecium bursaria. *Planta* 153,
575 481–485.

- 576 16. Sachs, J.L., and Simms, E.L. (2006). Pathways to mutualism breakdown. *Trends in*
577 *Ecology & Evolution* 21, 585–592.
- 578 17. Herre, E.A., Knowlton, N., Mueller, U.G., and Rehner, S.A. (1999). The evolution of
579 mutualisms: exploring the paths between conflict and cooperation. *Trends in Ecology &*
580 *Evolution* 14, 49–53.
- 581 18. Muggia, L., Nelson, P., Wheeler, T., Yakovchenko, L.S., Tønsberg, T., and Spribille, T.
582 (2011). Convergent evolution of a symbiotic duet: The case of the lichen genus
583 *Polychidium* (Peltigerales, Ascomycota). *American Journal of Botany* 98, 1647–1656.
- 584 19. Masson-Boivin, C., Giraud, E., Perret, X., and Batut, J. (2009). Establishing nitrogen-
585 fixing symbiosis with legumes: how many rhizobium recipes? *Trends in Microbiology*
586 17, 458–466.
- 587 20. Boscaro, V., Husnik, F., Vannini, C., and Keeling, P.J. (2019). Symbionts of the ciliate
588 *Euplotes*: diversity, patterns and potential as models for bacteria–eukaryote
589 endosymbioses. *Proceedings of the Royal Society B: Biological Sciences* 286, 20190693.
- 590 21. Hulcr, J., and Stelinski, L.L. (2017). The Ambrosia Symbiosis: From Evolutionary
591 Ecology to Practical Management. *Annual Review of Entomology* 62, 285–303.
- 592 22. Zagata, P., Greczek-Stachura, M., Tarcz, S., and Rautian, M. (2016). The Evolutionary
593 Relationships between Endosymbiotic Green Algae of *Paramecium bursaria* Syngens
594 Originating from Different Geographical Locations. *Folia Biologica* 64, 47–54.
- 595 23. Kadono, T., Kawano, T., Hosoya, H., and Kosaka, T. (2004). Flow cytometric studies of
596 the host-regulated cell cycle in algae symbiotic with green paramecium. *Protoplasma*
597 223, 133–141.
- 598 24. Soldo, A.T., Godoy, G.A., and Larin, F. (1978). Purine-Excretory Nature of Refractile
599 Bodies in the Marine Ciliate *Parauronema acutum**. *The Journal of Protozoology* 25,
600 416–418.
- 601 25. Shah, N., and Syrett, P.J. (1984). The uptake of guanine and hypoxanthine by marine
602 microalgae. *Journal of the Marine Biological Association of the United Kingdom* 64,
603 545–556.
- 604 26. Quispe, C.F., Sonderman, O., Khasin, M., Riekhof, W.R., Van Etten, J.L., and Nickerson,
605 K.W. (2016). Comparative genomics, transcriptomics, and physiology distinguish
606 symbiotic from free-living *Chlorella* strains. *Algal Research* 18, 332–340.
- 607 27. Minaeva, E., and Ermilova, E. (2017). Responses triggered in chloroplast of *Chlorella*
608 *variabilis* NC64A by long-term association with *Paramecium bursaria*. *Protoplasma*, 1–8.
- 609 28. Arnou, P., Oleson, J.J., and Williams, J.H. (1953). The Effect of Arginine on the
610 Nutrition of *Chlorella vulgaris*. *American Journal of Botany* 40, 100–104.
- 611 29. Maxwell, K., and Johnson, G.N. (2000). Chlorophyll fluorescence—a practical guide. *J*
612 *Exp Bot* 51, 659–668.

- 613 30. Esteban, G.F., Fenchel, T., and Finlay, B.J. (2010). Mixotrophy in Ciliates. *Protist* *161*,
614 621–641.
- 615 31. Stanley, G.D., and Lipps, J.H. (2011). Photosymbiosis: The Driving Force for Reef
616 Success and Failure. *The Paleontological Society Papers* *17*, 33–59.
- 617 32. Caron, D.A. (2016). Mixotrophy stirs up our understanding of marine food webs. *PNAS*
618 *113*, 2806–2808.
- 619 33. Boulotte, N.M., Dalton, S.J., Carroll, A.G., Harrison, P.L., Putnam, H.M., Peplow, L.M.,
620 and van Oppen, M.J. (2016). Exploring the *Symbiodinium* rare biosphere provides
621 evidence for symbiont switching in reef-building corals. *The ISME Journal* *10*, 2693–
622 2701.
- 623 34. Lefèvre, C., Charles, H., Vallier, A., Delobel, B., Farrell, B., and Heddi, A. (2004).
624 Endosymbiont Phylogenesis in the Dryophthoridae Weevils: Evidence for Bacterial
625 Replacement. *Mol Biol Evol* *21*, 965–973.
- 626 35. Yellowlees, D., Rees, T.A.V., and Leggat, W. (2008). Metabolic interactions between
627 algal symbionts and invertebrate hosts. *Plant, Cell & Environment* *31*, 679–694.
- 628 36. Berkelmans, R., and van Oppen, M.J.H. (2006). The role of zooxanthellae in the thermal
629 tolerance of corals: a ‘nugget of hope’ for coral reefs in an era of climate change.
630 *Proceedings of the Royal Society B: Biological Sciences* *273*, 2305–2312.
- 631 37. Rowan, R. (2004). Thermal adaptation in reef coral symbionts. *Nature* *430*, 742–742.
- 632 38. Kinzie, R.A., Takayama, M., Santos, S.R., and Coffroth, M.A. (2001). The Adaptive
633 Bleaching Hypothesis: Experimental Tests of Critical Assumptions. *The Biological*
634 *Bulletin* *200*, 51–58.
- 635 39. Ye, S., Bhattacharjee, M., and Siemann, E. (2019). Thermal Tolerance in Green Hydra:
636 Identifying the Roles of Algal Endosymbionts and Hosts in a Freshwater Holobiont
637 Under Stress. *Microb Ecol* *77*, 537–545.
- 638 40. Venn, A.A., Loram, J.E., and Douglas, A.E. (2008). Photosynthetic symbioses in
639 animals. *J Exp Bot* *59*, 1069–1080.
- 640 41. Cimino, M.A., Patris, S., Ucharm, G., Bell, L.J., and Terrill, E. (2018). Jellyfish
641 distribution and abundance in relation to the physical habitat of Jellyfish Lake, Palau.
642 *Journal of Tropical Ecology* *34*, 17–31.
- 643 42. Husnik, F., and McCutcheon, J.P. (2016). Repeated replacement of an intrabacterial
644 symbiont in the tripartite nested mealybug symbiosis. *PNAS* *113*, E5416–E5424.
- 645 43. Koga, R., and Moran, N.A. (2014). Swapping symbionts in spittlebugs: evolutionary
646 replacement of a reduced genome symbiont. *The ISME Journal* *8*, 1237–1246.
- 647 44. Matsuura, Y., Moriyama, M., Łukasik, P., Vanderpool, D., Tanahashi, M., Meng, X.-Y.,
648 McCutcheon, J.P., and Fukatsu, T. (2018). Recurrent symbiont recruitment from fungal
649 parasites in cicadas. *PNAS* *115*, E5970–E5979.

- 650 45. Sepp, S.-K., Davison, J., Jairus, T., Vasar, M., Moora, M., Zobel, M., and Öpik, M.
651 (2019). Non-random association patterns in a plant–mycorrhizal fungal network reveal
652 host–symbiont specificity. *Molecular Ecology* 28, 365–378.
- 653 46. Parker, B.J., Hrček, J., McLean, A.H.C., and Godfray, H.C.J. (2017). Genotype
654 specificity among hosts, pathogens, and beneficial microbes influences the strength of
655 symbiont-mediated protection. *Evolution* 71, 1222–1231.
- 656 47. Stein, J.R. (1979). (ED.) *Handbook of Phycological Methods: Culture Methods and*
657 *Growth Measurements* (Cambridge University Press).
- 658 48. Shen, S. (2008). Genetic diversity analysis with ISSR PCR on green algae <Emphasis
659 Type="Italic">*Chlorella vulgaris*</Emphasis> and <Emphasis Type="Italic">*Chlorella*
660 *pyrenoidosa*</Emphasis>. *Chin. J. Ocean. Limnol.* 26, 380–384.
- 661 49. Schneider, C.A., Rasband, W.S., and Eliceiri, K.W. (2012). NIH Image to ImageJ: 25
662 years of image analysis. *Nature Methods*. Available at:
663 <https://www.nature.com/articles/nmeth.2089> [Accessed May 7, 2018].
- 664 50. Oxborough, K., Moore, C.M., Suggett, D.J., Lawson, T., Chan, H.G., and Geider, R.J.
665 (2012). Direct estimation of functional PSII reaction center concentration and PSII
666 electron flux on a volume basis: a new approach to the analysis of Fast Repetition Rate
667 fluorometry (FRRf) data. *Limnology and Oceanography: Methods* 10, 142–154.
- 668 51. McKew, B.A., Davey, P., Finch, S.J., Hopkins, J., Lefebvre, S.C., Metodiev, M.V.,
669 Oxborough, K., Raines, C.A., Lawson, T., and Geider, R.J. (2013). The trade-off between
670 the light-harvesting and photoprotective functions of fucoxanthin-chlorophyll proteins
671 dominates light acclimation in *Emiliania huxleyi* (clone CCMP 1516). *New Phytologist*
672 200, 74–85.
- 673 52. Benton, H.P., Want, E.J., and Ebbels, T.M.D. (2010). Correction of mass calibration gaps
674 in liquid chromatography-mass spectrometry metabolomics data. *Bioinformatics* 26,
675 2488–2489.
- 676 53. Smith, C.A., Want, E.J., O’Maille, G., Abagyan, R., and Siuzdak, G. (2006). XCMS:
677 Processing Mass Spectrometry Data for Metabolite Profiling Using Nonlinear Peak
678 Alignment, Matching, and Identification. *Anal. Chem.* 78, 779–787.
- 679 54. Tautenhahn, R., Böttcher, C., and Neumann, S. (2008). Highly sensitive feature detection
680 for high resolution LC/MS. *BMC Bioinformatics* 9, 504.
- 681 55. Touw, W.G., Bayjanov, J.R., Overmars, L., Backus, L., Boekhorst, J., Wels, M., and van
682 Hijum, S.A.F.T. (2013). Data mining in the Life Sciences with Random Forest: a walk in
683 the park or lost in the jungle? *Brief. Bioinformatics* 14, 315–326.
- 684 56. Hopkins, D.P., Cameron, D.D., and Butlin, R.K. (2017). The chemical signatures
685 underlying host plant discrimination by aphids. *Scientific Reports* 7, 8498.
- 686 57. Warnes, G.R., Bolker, B., Bonebakker, L., Gentleman, R., Huber, W., Liaw, A., Lumley,
687 T., Maechler, M., Magnusson, A., and Moeller, S. (2009). *gplots: Various R*
688 *programming tools for plotting data. R package version 2, 1.*

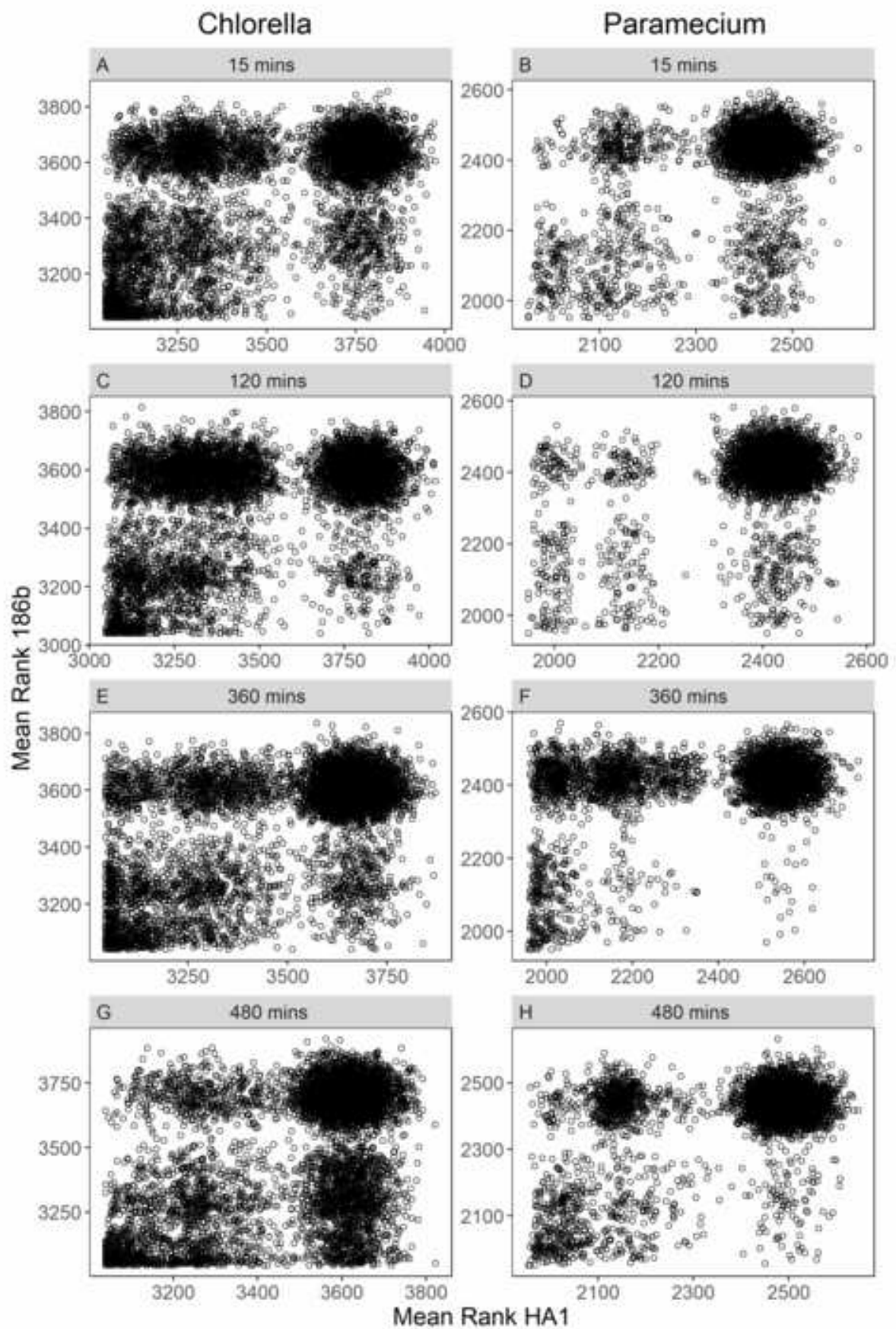
- 689 58. Storey, J.D., and Tibshirani, R. (2003). Statistical significance for genomewide studies.
690 PNAS *100*, 9440–9445.
- 691 59. Kaefer, A., Lingner, T., Feussner, K., Göbel, C., Feussner, I., and Meinicke, P. (2009).
692 MarVis: a tool for clustering and visualization of metabolic biomarkers. BMC
693 Bioinformatics *10*, 92.
- 694 60. Kanehisa, M., and Goto, S. (2000). KEGG: kyoto encyclopedia of genes and genomes.
695 Nucleic Acids Res. *28*, 27–30.
- 696 61. Kanehisa, M., Sato, Y., Furumichi, M., Morishima, K., and Tanabe, M. (2019). New
697 approach for understanding genome variations in KEGG. Nucleic Acids Res. *47*, D590–
698 D595.
- 699 62. Caspi, R., Billington, R., Fulcher, C.A., Keseler, I.M., Kothari, A., Krummenacker, M.,
700 Latendresse, M., Midford, P.E., Ong, Q., Ong, W.K., *et al.* (2018). The MetaCyc
701 database of metabolic pathways and enzymes. Nucleic Acids Res *46*, D633–D639.
- 702 63. R Core Team (2018). R: A Language and Environment for Statistical Computing.
703 Available at: <https://www.R-project.org/>.
- 704 64. Wickham, H. (2016). ggplot2: Elegant Graphics for Data Analysis.
- 705 65. Pinheiro, J., Bates, D., DebRoy, S., Sarkar, D., and R core Team (2019) (2019). nlme:
706 Linear and Nonlinear Mixed Effects Models. Available at: [https://CRAN.R-](https://CRAN.R-project.org/package=nlme)
707 [project.org/package=nlme](https://CRAN.R-project.org/package=nlme).
- 708
- 709
- 710
- 711
- 712

KEY RESOURCES TABLE

REAGENT or RESOURCE	SOURCE	IDENTIFIER
Bacterial and Virus Strains		
<i>Serratia marscesens</i>	Collection of Institut Pasteur	CIP 103235T
Chemicals, Peptides, and Recombinant Proteins		
Protozoan Pellet Media	Carolina Biological Supply	132360
Paraquat dichloride	Sigma-Aldrich	36541; CAS: 75365-73-0
8-peak rainbow calibration particles	BioLegend	422903
Chelex100 resin	Bio-Rad Laboratories	1421253
Deposited Data		
Mass spectrometry data, fluorimetry data and flow cytometry data	This paper	DOI: 10.17632/6zspctmwpj.1
Experimental Models: Organisms/Strains		
<i>P. bursaria</i> – <i>Chlorella</i> 186b strain	Culture Collection of Algae and Protozoa	CCAP 1660/18
<i>P. bursaria</i> – <i>Chlorella</i> HA1 strain	National BioResource project	NBRP ID: PB034004A
Oligonucleotides		
ISSR primer '65': AGAGAGAGAGAGAGGCC	[48]	N/A
Software and Algorithms		
ImageJ v1.50i	[49]	https://imagej.nih.gov/ij/
xcms R package	[52–54]	https://bioconductor.org/packages/release/bioc/html/xcms.html
MarVis-Suite 2.0 software	[59]	http://marvis.gobics.de/

Figure 1

[Click here to access/download;Figure;Figure 1.tif](#)



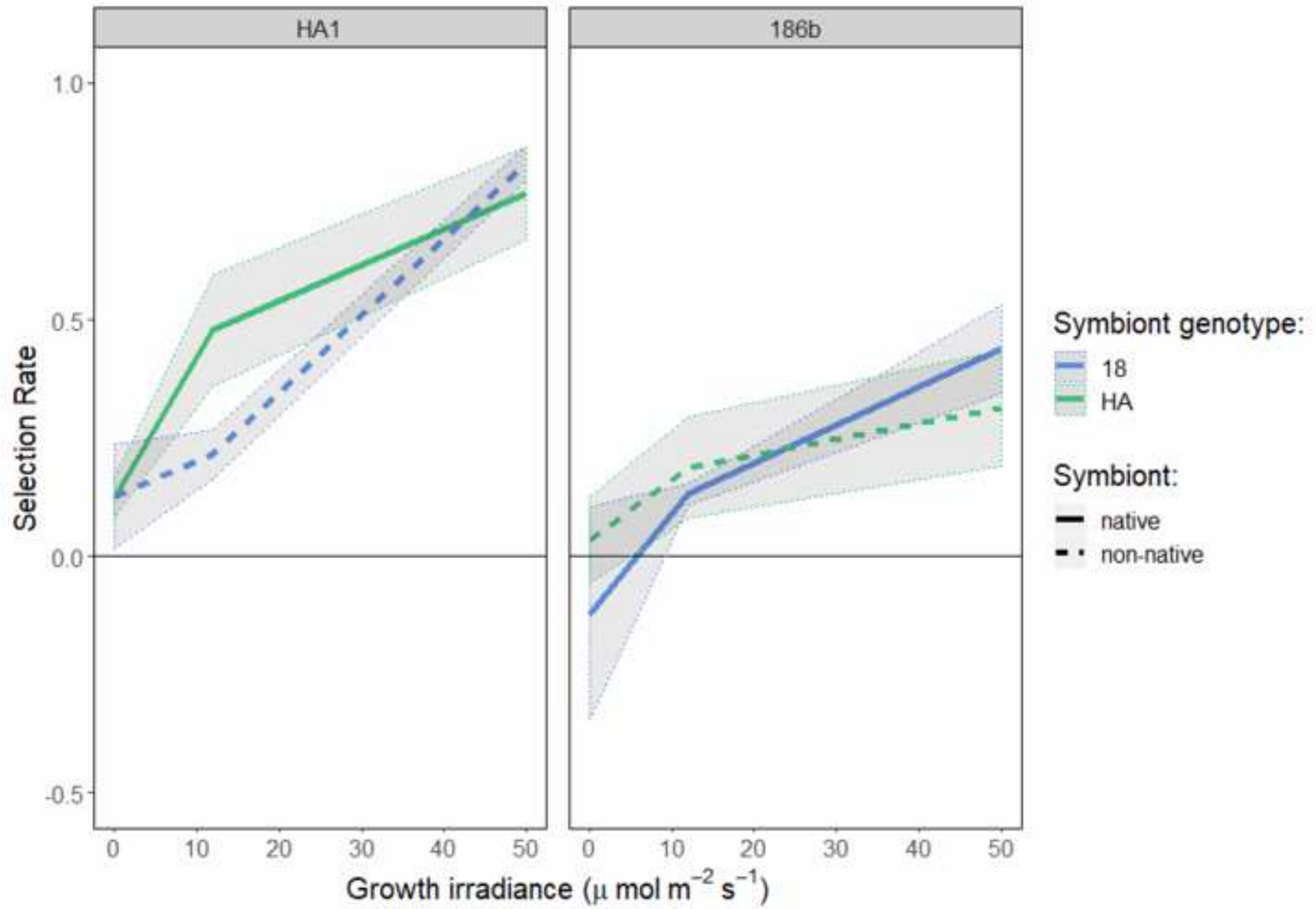
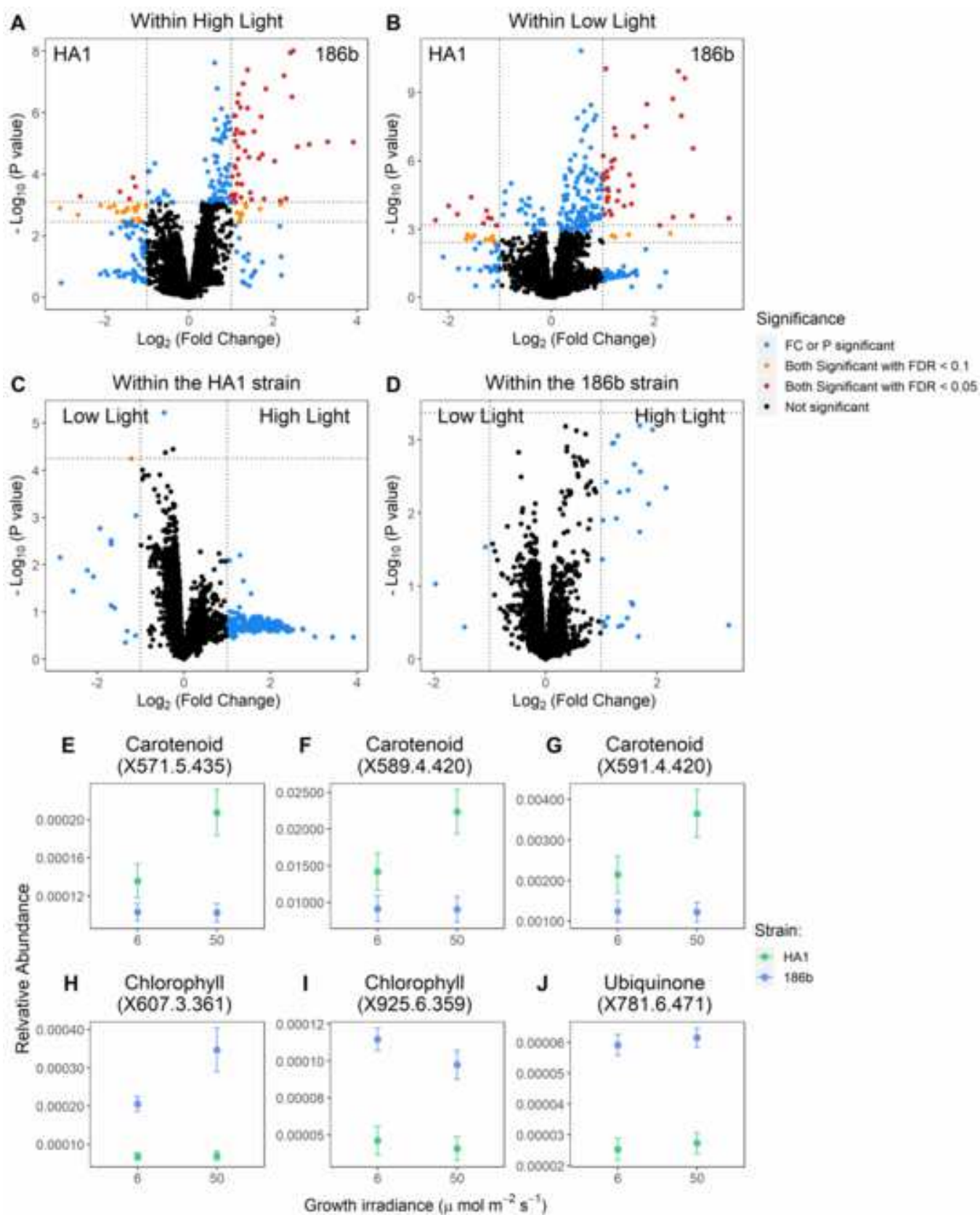
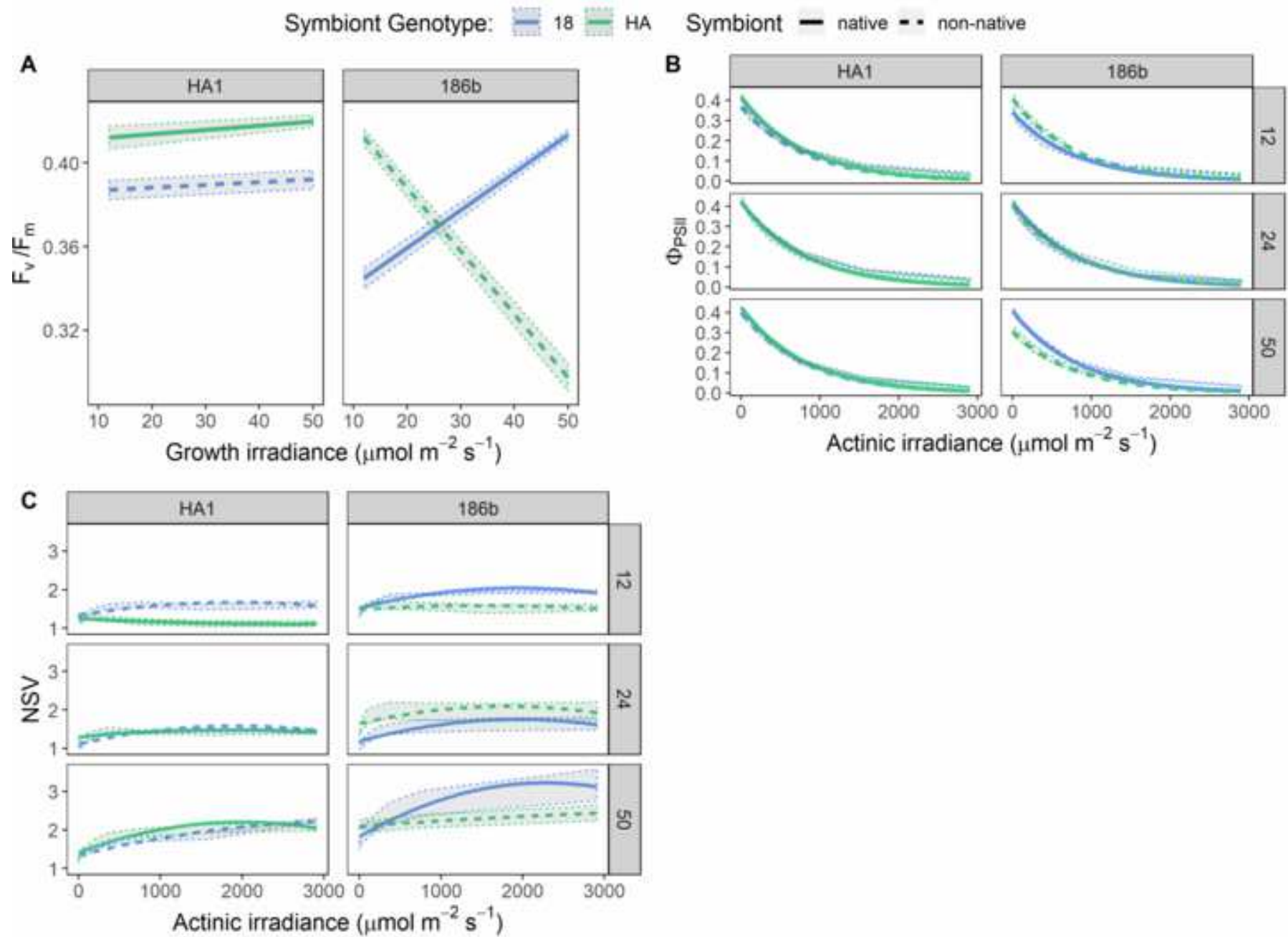


Figure 3

[Click here to access/download;Figure;Figure 3.tif](#)





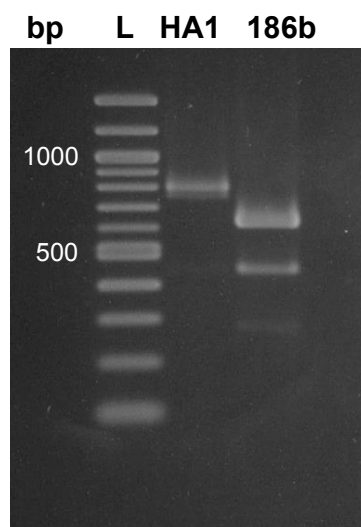


Figure S1: Diagnostic PCR between the HA1 and 186b *Chlorella* strains.

Related to STAR Methods.

Showing clear banding pattern differences with the '65 ISSR' primer. Shown with a 100 bp ladder.

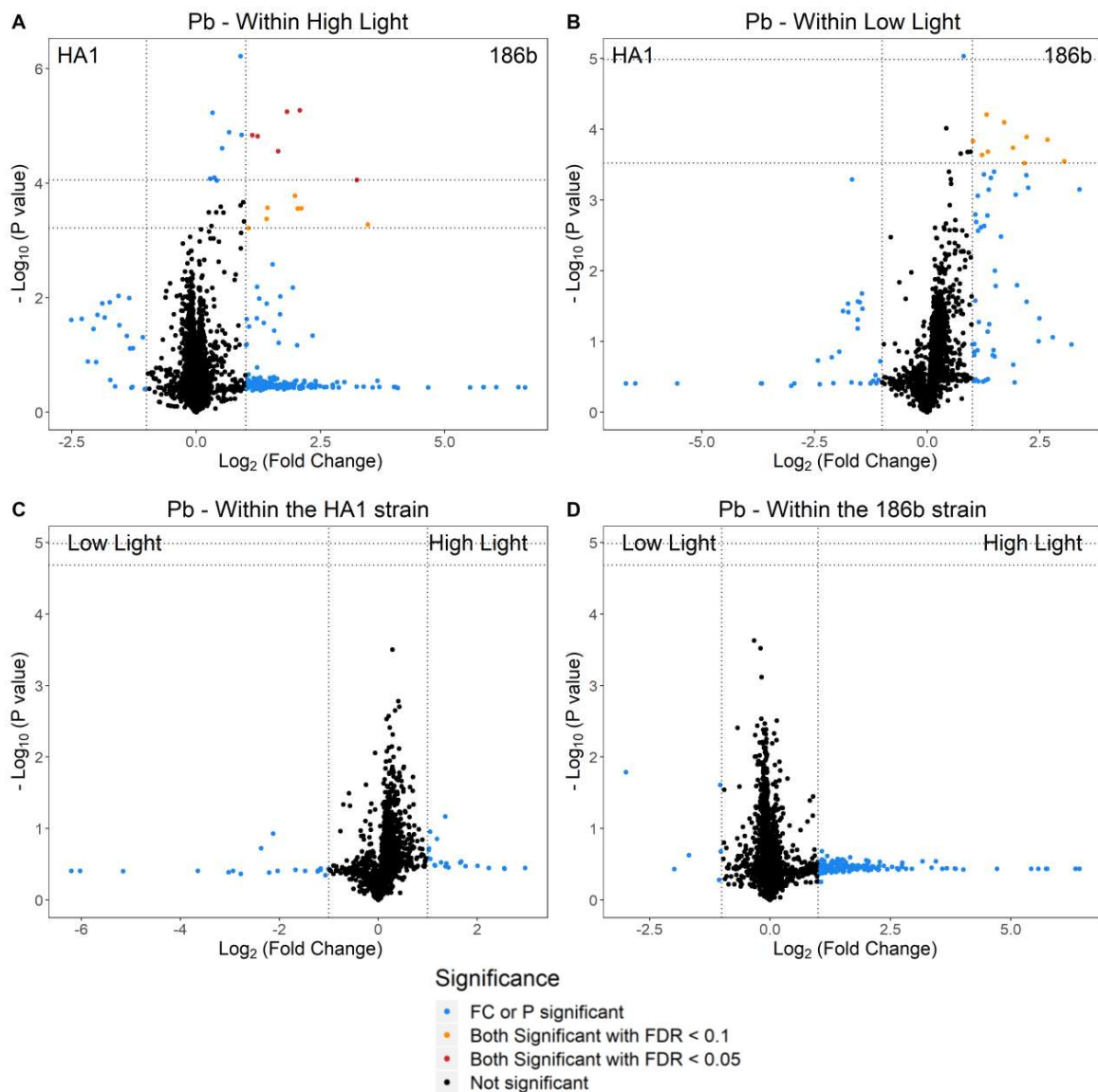


Figure S2: Comparisons of the unlabelled *Paramecium* metabolites between the strains and light conditions. Related to the main text and Figure 3.

Volcano plots for the unlabelled *Paramecium* metabolite comparisons. Plotting the fold change of each metabolite against its statistical significance. The data points are highlighted at two false discovery rate (FDR) values, and if the $\text{Log}_2(\text{fold change})$ is greater than 1 or less than -1. A.) Comparing the expression between the two strains within the high light condition. B.) Comparing the expression between the two strains within the low light condition. C.) Comparing expression between the two light levels within the HA1 strain. D.) Comparing expression between the two light levels within the 186b strain. See Table S4 for the identified significant metabolites.

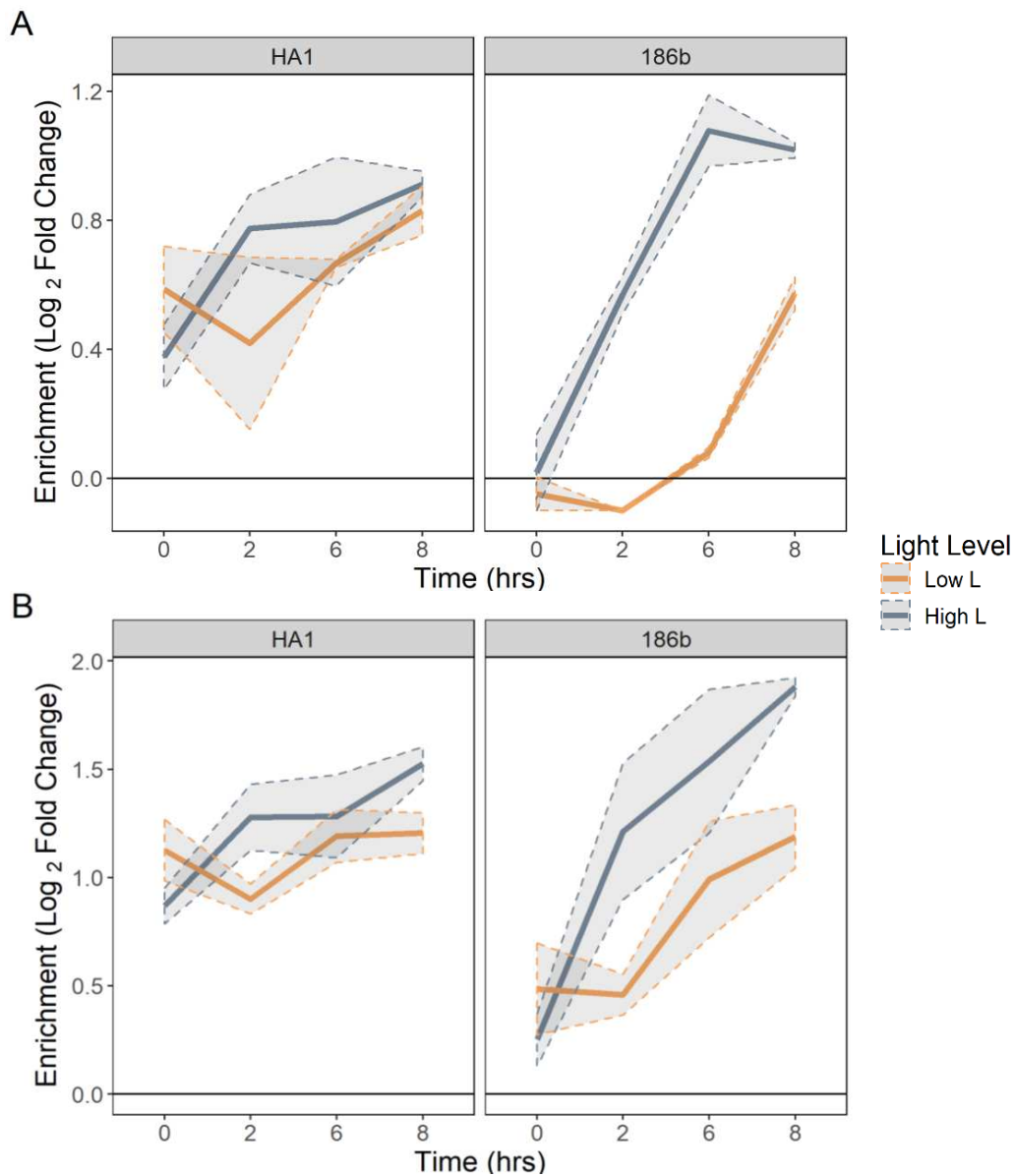


Figure S3: The interaction of light intensity and strain identity on the C¹³ enrichment profile of carbohydrate metabolites in the *Paramecium* fraction. Related to the main text and STAR Methods.

For all panels, the enrichment value is the Log₂ of the Fold Change in enrichment of the C¹³ labelled fraction compared to the control. Presented as the mean (n=3) ±SE. The low light level refers to 6 μmol m⁻² s⁻¹ and the high light to 50 μmol m⁻² s⁻¹. A) Profile of 689.2 m/z, 16 rt, Glycogen. B) Profile of 365.1 m/z, 16 rt, a disaccharide, thought to be sucrose.

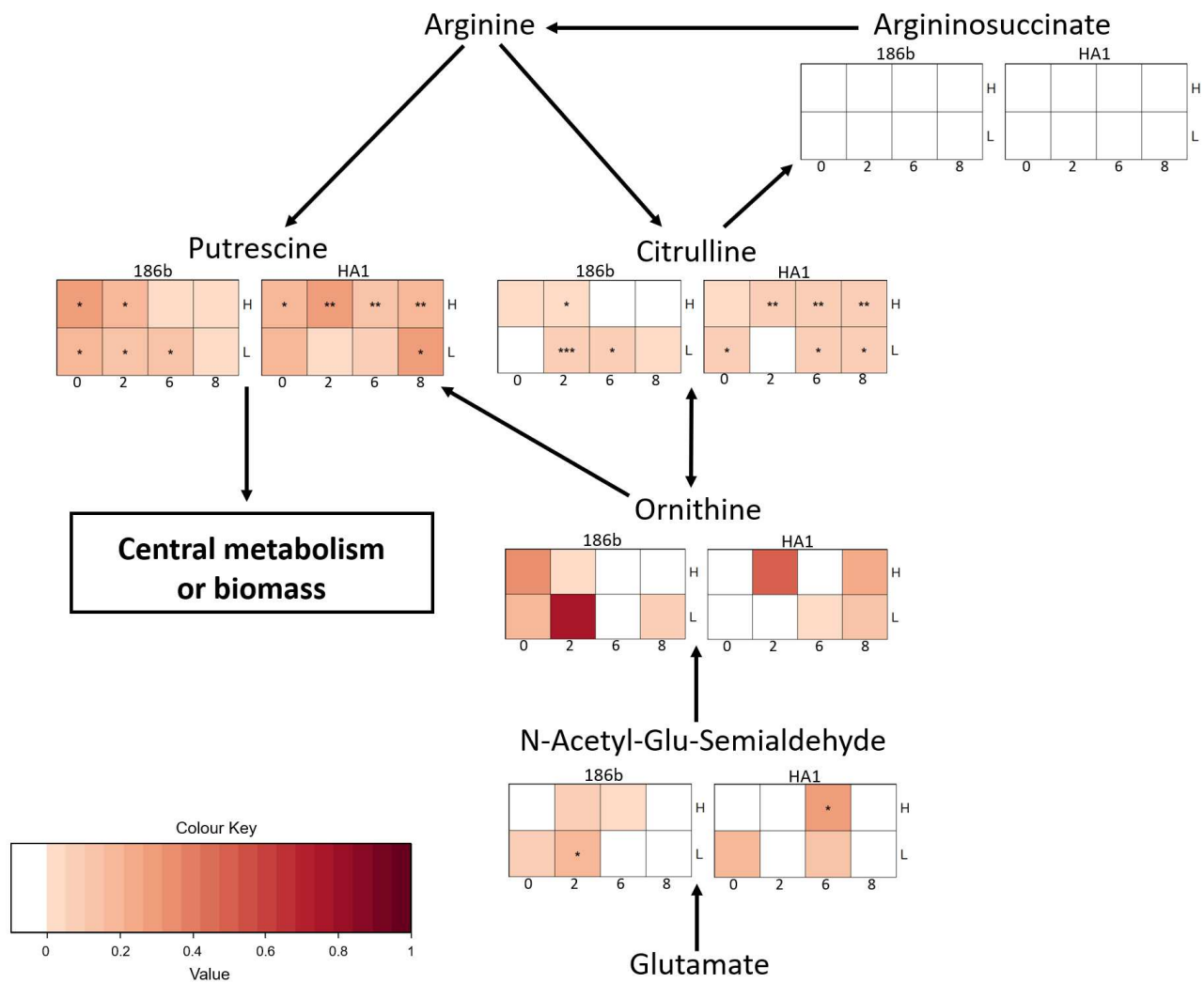


Figure S4: Schematic pathway diagram of nitrogen enrichment in the amino acid metabolism of the *Chlorella* metabolic fraction. Related to the main text and STAR methods.

The tables show relative N^{15} enrichment across time (in hrs), in the two light conditions (H = $50 \mu\text{mol m}^{-2} \text{s}^{-1}$, L = $6 \mu\text{mol m}^{-2} \text{s}^{-1}$). The colour corresponds to the fold change of the enrichment compared to the control, with significance stars indicating the statistical strength of this change. The nitrogen enrichment is focused downstream from arginine; ornithine, putrescine and citrulline possessed clear enrichment profiles while upstream compounds such as arginosuccinate had no detectable enrichment. This analysis is further explained in the STAR methods section.

Strain	Year	Location	Latitude and Longitude	Elevation	Average Temperature Range	Average Total Sunshine hours a year	Culture Collection
186b	2006	Lilly Loch, Inverawe, Scotland, UK	56°26'03.8"N 5°12'22.1"W	20-40m	2.3°C to 17.9°C ¹	1,219.4 hrs ¹	CCAP 1660/18 ²
HA1	2010	Hirosaki-city, Aomori pref, Japan	40°35'35.02"N 140°28'21"E	45m	-5°C to 28°C ³	2013.2 hrs ³	NBRP ID: PB034004A ⁴

Table S1. Details of the *P. bursaria* – *Chlorella* strains. Related to main text and STAR Methods.

¹ Based on the Met Office UK Climate averages data for Dunstaffnage (<https://www.metoffice.gov.uk/research/climate/maps-and-data/uk-climate-averages>)

² https://www.ccap.ac.uk/strain_info.php?Strain_No=1660/18

³ Based on data for Hirosaki city and Aomori airport (<https://www.japanhoppers.com/en/tohoku/hirosaki/weather/>) (<https://www.worldweatheronline.com/hirosaki-weather-averages/aomori/jp.aspx>)

⁴ http://nbrpcms.nig.ac.jp/paramecium/wp-content/themes/paramecium/data/strain_ha1g.pdf

RF Time	Detected Mass	Retention Time	Pathway	Candidate Compounds	Exact Mass	Adduct	KEGG/ MetaCyc
1	113	482	Pyrimidine/Amino acid	Uracil	112.0273	H+	C00106
				1,3-diaminopropane	74.0844	K+	C00986
1	166	478	Purine	5-Amino-4-imidazole carboxylate	127.0382	K+	C05516
1,2	237.1	286	Biotin	Dethiobiotin	214.1317	Na+	C01909
1,2,3,4	871.6	405	Chlorophyll	Pheophytin A	870.5659	H+	C05797
1,2,4	593.3	405	Chlorophyll	Pheophorbide A	592.2686	H+	C18021
				Urobilinogen	592.3261	H+	C05790
2,3	140	213	Amino acid	L-Aspartate 4-semialdehyde	117.0426	Na+	C00441
				Indole	117.0578	Na+	C00463
				1-Aminocyclopropane-carboxylate	101.0477	K+	C01234
				5-Aminopentanal	101.0841	K+	C12455
3	482.4	324	Folate biosynthesis	Dihydrofolate	443.1553	K+	C00415
3	848.6	294	Ubiquinone	Rhodoquinone-10	847.6842	H+	CPD-9613
4	227.1	460	Amino acid/Chlorophyll	Tryptophan	204.0899	Na+	C00078
				Porphobilinogen	226.0954	H+	C00931

Table S2. List of metabolite IDs found to be co-enriched with ^{15}N in the *Chlorella* fraction and their candidate identifications. Related to Figure 1, the main text and STAR Methods.

RF Time	Detected Mass	Retention Time	Pathway	Candidate Compounds	Exact Mass	Adduct	KEGG
1	100	16	Glycerophospholipid	Ethanolamine	61.0528	K+	C00189
1	689.2	16	Carbohydrate	Glycogen	666.2219	Na+	C00182
1,2	124	15	Vitamins and Cofactors	Niacin	123.032	H+	C00253
1,2	261	14	Carbohydrate	Monosaccharide phosphate	260.0297	H+	C00092
1,2,3	251	17	Isoprenoid pathway	(R)-5-Phosphomevalonate	228.0399	Na+	C01107
1,2,3,4	190	341	Phosphonate	Demethylphosphinothricin	167.0347	Na+	C17962
1,2,3,4	441.3	310	Lipid	Hydroxycholesterol	402.3498	K+	C05500
1,2,3,4	639.2	414	Heme biosynthesis	Haem	616.1773	Na+	C00032
1,2,3,4	212.9	479	Chlorocyclohexane and chlorobenzene degradation	Chlorodienelactone	173.972	Ka+	C04706
1,2,4	109	479	Quinone	p-Benzoquinone	108.0211	H+	C00472
1,2,4	345.9	480	Amino acid metab	3-Iodo-L-tyrosine	306.9705	K+	C02515
1,3,4	169	19	Central metabolism	2-Oxoglutarate	146.0215	Na+	C00026
				2-Oxoisocaproate	130.063	K+	C00233
				3-Methyl-2-oxopentanoate	130.063	K+	C00671
				2-Dehydropantoate	146.0579	K+	C00966
				3-Phosphonopyruvate	167.9824	H+	C02798
				Phosphoenolpyruvate	167.9824	H+	C00074
2	313.2	287	Lipid	HPODE	312.2301	H+	C04717
2,3,4	519.1	400	Peptide	Nitro-hydroxy-glutathionyl-dihydronaphthalene	496.1264	Na+	C14803
2,4	71.1	373	Amino acid	Aminopropionitrile	70.0531	H+	C05670
3	405.1	236	Isoprenoid pathway	Farnesyl diphosphate	382.131	Na+	C00448

Table S3. List of metabolite IDs found to be co-enriched with ^{13}C in the *P. bursaria* fraction and their candidate identifications. Related to Figure 1, the main text and STAR Methods.

Fraction	Upregulated in	Condition	Detected Mass	Retention Time	FDR	Pathway	Candidate Compounds	Exact Mass	Adduct	Kegg / Metacyc	
Chlorella	HA1 strain	H & L light	247.2	336	*,**	Alkaloid/quinone	Anapheline	224.1889	Na+	C06183	
							Geranylhydroquinone	246.162	H+	C10793	
				283.3	336	*,**	Fatty acid	Oleate	282.2559	H+	C00712
		H light	218.2	17	*	Amino acid	L-Glutamylputrescine	217.1426	H+	C15699	
							Alanyl-L-lysine	217.1426	H+	C05341	
				265.3	337	*	Fatty acid	1-Hexadecanol	242.261	Na+	C00823
				385.2	375	*	Plant Hormone	Gibberellin A36	362.1729	Na+	C11862
				571.5	435	*	Carotenoid	Methoxyneurosporene	570.4801	H+	C15895
				589.4	420	*	Carotenoid	Echinenone	550.4175	K+	C08592
			Anhydrorhodovibrin					566.4488	Na+	C15877	
			Hydroxychlorobactene					550.4175	K+	C15911	
		3-Hydroxyechinenone	566.4124					Na+	C15966		
			591.4	420	*	Carotenoid	Zeaxanthin	568.428	Na+	C06098	
							Zeinoxanthin	552.4331	K+	C08590	
					beta-Cryptoxanthin		552.4331	K+	C08591		
					Xanthophyll		568.428	Na+	C08601		
Low Light	HA1 strain		743.5	373	*	Phosphoglyceride	1-18:3-2-trans-16:1-phosphatidylglycerol	742.4785	H+	CPD-2186	
186 Strain	H & L light	105	15	*,**	Central metabolism	Hydroxypyruvate	104.011	H+	C00168		
						Allophanate	104.0222	H+	C01010		
		169	17	**	Central metabolism	2-Oxoglutarate	146.0215	Na+	C00026		
						Phosphoenolpyruvate	167.9824	H+	C00074		
						3-Phosphonopyruvate	167.9824	H+	C02798		
						2-Oxoisocaproate	130.063	K+	C00233		
						3-Methyl-2-oxopentanoate	130.063	K+	C00671		
						2-Dehydropantoate	146.0579	Na+	C00966		
						Coumarin	146.0368	Na+	C05851		
				273.2	395	**	Fatty Acid	16-Hydroxypalmitate	272.2351	H+	C18218
		289.3	244	**	Diterpenoid	Kaurenol	288.2453	H+	C11872		

Fraction	Upregulated in	Condition	Detected Mass	Retention time	FDR	Pathway	Candidate Compounds	Exact mass	Adduct	KEGG
Chlorella			337.3	380	**	Fatty acids	13;16-Docosadienoic acid	336.3028	H+	C16533
			607.3	361	**	Chlorophyll	Protoporphyrinogen IX	568.305	K+	C01079
			781.6	471	**	Ubiquinone	3-methoxy-4-hydroxy-5-nonaprenylbenzoate	780.2	H+	CPD-9898
			925.6	359	**	Chlorophyll	Bacterio-pheophytins	888.5765	K+	C05798
		H light	262.1	248	**	Folate	Dihydrobiopterin	239.1018	Na+	C00268
							6-Lactoyl-5;6;7;8-tetrahydropterin	239.1018	Na+	C04244
			323.2	248	*	Photoreception	Vitamin A aldehyde	284.214	K+	C00376
			335.3	372	**	Isoprenoids	Phytol	296.3079	K+	C01389
			751.5	366	**	Ubiquinone	Octaprenyl-methyl-hydroxy-methoxy-1;4-benzoquinone	712.5431	K+	C05815
		L light	273.3	268	**	Diterpenoid	Ent-Kaurene	272.2504	H+	C06090
P. bursaria 186 strain	H & L light	124	238	**,*	Vitamins and Cofactors	Niacin	123.032	H+	C00253	
		126	217	**,*	Sulfur metabolism	Taurine	125.0147	H+	C00245	
		170	237	**,*	Amino acid	Glutamate	147.0532	Na+	C00025	
						5-Amino-4-oxopentanoate	131.0582	K+	C00430	
						Glutamate 5-semialdehyde	131.0582	K+	C01165	
		364.2	236	*,*	Antibiotic ?	ACV	363.1464	H+	C05556	
	396.1	237	*,*	Antibiotic ?	Deacetylcephalosporin C	373.0944	Na+	C03112		
					Novobiocic acid	395.1369	H+	C12474		
		H light	352.2	237	*	Plant hormone?	trans-Zeatin riboside	351.1543	H+	C16431
			390.1	237	*	Amino/nucleotide sugar	N-Acetylneuraminate 9-phosphate	389.0723	H+	C06241
			416.1	250	**	Antibiotic ?	Cephalosporin C	415.1049	H+	C00916
							Chlorobiocic acid	415.0823	H+	C12471
			434.1	249	*	Antibiotic ?	Novobiocic acid	395.1369	K+	C12474
		L light	418.2	268	*	Sphingolipid	Sphingosine 1-phosphate	379.2488	K+	C06124

Table S4. The metabolite IDs and candidate identification for the metabolites of interest from the unlabelled metabolic analyses. Related to Figure 3, Figure S2, and the main text.

These metabolites were therefore upregulated in either one of the strains or in one of the light conditions. This table includes both the *Chlorella* and *P. bursaria* results.